Z. Kristallogr. **220** (2005) 704–711

Crossover from classical to 3d-Ising critical behaviour near the antiferrodistortive phase transition of lawsonite

Wilfried Schranz*,[I], Andreas Tröster[I], Manuel Gardon[I], Gerhard Krexner[I], Manfred Prem[I], Michael Allan Carpenter[II], Peter Sondergeld[II] and Thomas Armbruster[III]

[I] Institut für Experimentalphysik, Universität Wien, Strudlhofgasse 4, 1090 Wien, Austria
[II] Department of Earth Sciences, University of Cambridge, Downing Street, Cambridge CB2 3EQ, UK
[III] Laboratorium für chemische und mineralogische Kristallographie, Universität Bern, Freiestraße 3, 3012, Bern, Switzerland

Received June 6, 2004; accepted September 30, 2004

Lawsonite / Precursor / Landau-Ginzburg-model / 3-d Ising / Crossover / Phase transitions

Abstract. Results of X-ray scattering intensities and peak profiles of lawsonite single crystals are presented in a wide temperature range including the antiferrodistortive phase transition $Cmcm - (T_c \approx 270\ \mathrm{K}) \rightarrow Pmcn$. In the integrated intensities of the superlattice reflections above T_c pronounced pretransitional tails similar to those detected recently in birefringence [P. Sondergeld *et al.*, Phys. Rev. B**62**, 6143 (2000)] and in excess entropy data [S. A. Hayward *et al.*, Eur. J. Min. **14**, 1145 (2002)] are observed. These tails correspond to diffuse Lorentzian shaped scattering peaks. The temperature variation of the diffuse scattering intensity and profile can be well described within a Landau-Ginzburg model. In combination with entropy data we obtain a complete set of free energy parameters. Using these coefficients we are able to fit the spontaneous part and the precursor tails of the integrated intensities, the excess birefringence and entropy in a broad temperature range outside a temperature interval of about ± 3 K around T_c. In the vicinity of T_c the experimental data are in excellent agreement with the predictions of a crossover model, the effective critical exponent $\alpha_{\mathrm{eff}}(\tau)$ varying from the classical ($\alpha_{\mathrm{eff}} = 0.5$) to the 3d Ising limit ($\alpha_{\mathrm{eff}} = 0.11$). Lawsonite therefore represents an ideal system to study the crossover from classical to critical behavior.

1. Introduction

Lawsonite, $CaAl_2[Si_2O_7](OH)_2 \cdot H_2O$, is a mineral with a wide P-T stability field (Schmidt, 1995) of about 8.5 GPa-1170 K. Containing ≈11 wt% H_2O in the structure, it may carry water down to depth beyond vulcanic arcs of 250 km into Earth's mantle at subduction zones (Schmidt and Poli, 1998). It is therefore regarded as an essential component in the geological water cycle.

The protons also play a prominent role in the two consecutive phase transitions at $T_c \approx 270$ K and $T_2 \approx 120$ K, which lead the crystal from the space group *Cmcm* via *Pmcn* to $P2_1cn$, as both transitions involve a combination of hydrogen motions and local distortions of the silicate framework (Baur, 1978; Libowitzky and Armbruster, 1995; Libowitzky and Rossman, 1996). The phase transition $Cmcm \rightarrow Pmcn$ occurs within the same crystal class. It is related to an instability at the Brillouin zone boundary, i.e. can be classified (Sondergeld *et al.*, 2000) as antiferrodistortive. Below $T_2 = 120$ K the structure changes to the polar space group $P2_1cn$, accompanied by ferroelectric hysteresis loops (Sondergeld *et al.*, 2001). Thus Lawsonite represents one of the rare examples of a ferroelectric mineral. Moreover the thermodynamic properties like dielectric permittivity, spontaneous strain or birefringence near the ferroelectric phase transition can be unambigously fitted by a classical Landau 2–4 potential (Sondergeld *et al.*, 2001; Sondergeld *et al.*).

In contrast to the ferroelectric phase transition, the antiferrodistortive phase transition at $T_c = 270$ K is accompanied by huge precursor tails (Sondergeld *et al.*, 2000). To gain more insight into the origin of these tails we performed X-ray measurements of the superstructure reflections and the diffuse scattering around these peaks in the vicinity of the antiferrodistortive phase transition. As a result, we observe that the superlattice intensities, birefringence and excess entropy (Martin-Olalla *et al.*, 2001; Hayward *et al.*, 2002) data reveal a strikingly similar temperature dependence. Moreover, the phase transition shows "non-classical" behaviour in the following sense: In a broad temperature range outside an interval of a few Kelvin around T_c, the data can be well described by a Landau-Ginzburg theory including small fluctuation corrections implying classical critical exponents $\gamma = 1$, $\nu = {}^1/_2$, $\alpha = {}^1/_2$. When approaching T_c further, the fluctuations become too large and the system does not longer follow this simple classical behaviour.

2. Experimental

2.1 Samples

For the present X-ray investigation we used pieces from sample no. A7331 of the National History Museum, Bern

* Correspondence author (e-mail: schranz@ap.univie.ac.at)

originating from Reed Ranch, Tiburon, California. Prompt Gamma Activation Analysis (PGAA) on two samples revealed slightly different but close to ideal compositions, i.e. $Ca_{0.975}Al_{1.99}Fe_{0.0075}Ti_{0.00162}[Si_{1.995}O_7](OH)_2 \cdot H_2O$ and $Ca_{1.005}Al_{1.855}Fe_{0.0087}Ti_{0.0062}[Si_{2.1}O_7](OH)_2 \cdot H_2O$. Birefringence measurements were carried out on samples from Tiburon Peninsula, Marin County, California (No. G14555 of the South Australian Museum, Adelaide). The chemical composition was found to be close to ideal $CaAl_2[Si_2O_7](OH)_2 \cdot H_2O$, i.e. $Ca_{0.981}Al_{1.953}Fe_{0.036}Ti_{0.0132}[Si_{2.013}O_7](OH)_2 \cdot H_2O$. The calorimetric measurements (Hayward *et al.*, 2002; Martin-Olalla *et al.*, 2001) and neutron powder diffraction experiments (Carpenter *et al.*, 2003) were performed on samples from Valley Ford, California (no. 120943) of the Harvard University mineral collection. Electron microprobe analyses yielded the composition of lawsonite as $CaAl_{1.95}Fe_{0.05}[Si_2O_7](OH)_2 \cdot H_2O$.

2.2 X-ray diffraction

A single-crystal fragment of lawsonite with diameter of about 0.25 mm was measured on an Enraf-Nonius CAD4 four-circle diffractometer using MoK_α radiation with $\lambda = 0.71069$ Å. The temperature of the crystals was controlled using a commercial cooling device with an open nitrogen gas flow and a Cu−CuNi thermocouple in the vicinity of the sample. The temperature calibration procedure included two absolute reference points at 77 K and 295 K, respectively. Temperature dependent X-ray intensities of selected reflections were measured using ω-scan technique. The accuracy in temperature was +/−2 K. 10 of the strongest superstructure reflections fulfilling the (*hkl*)-condition $h + k = 2n + 1$ were chosen to study the evolution of long range order in the *Pmcn*-phase of lawsonite. 14 reflections, broadly distributed through reciprocal space, were used to determine the orientation matrix of the crystal. At each temperature of detection, the orientation matrix was redetermined first, then the intensities and profiles (ω-scans) were measured.

2.3 Birefringence measurements

The crystals were oriented according to the natural faces (morphology) and checked optically for macroscopic defects, inclusions, etc. Small and thin regions of the crystals free from fissures and inclusions with sample dimensions of $0.4–0.8 \times 2 \times 2\ mm^3$ were chosen. A polarizing microscope (Zeiss Axiophot) equipped with a Linkam hot stage was used for the optical experiments. The birefringence was measured (Sondergeld *et al.*, 2000) fully automatically using the Senarmont compensation method (Zimmermann and Schranz, 1993).

3. Experimental results

Fig. 1 shows the measured temperature dependence of the integrated intensities of 10 of the strongest superstructure reflections. A calculation of the structure factors using the X-ray refined structures (Libowitzky and Armbruster, 1995) reproduces correctly the experimentally obtained sequence of intensities (Fig. 1). Fig. 2 shows the superstructure peaks normalized at $T = 150$ K. One observes that they scale rather well. We have also calculated the temperature dependence of the structure factor of the (0 1 7)-peak as an example using the measured temperature dependent atomic positions of Meyer *et al.* (2001), yielding perfect agreement with the measured superlattice intensity (open circles in Fig. 1).

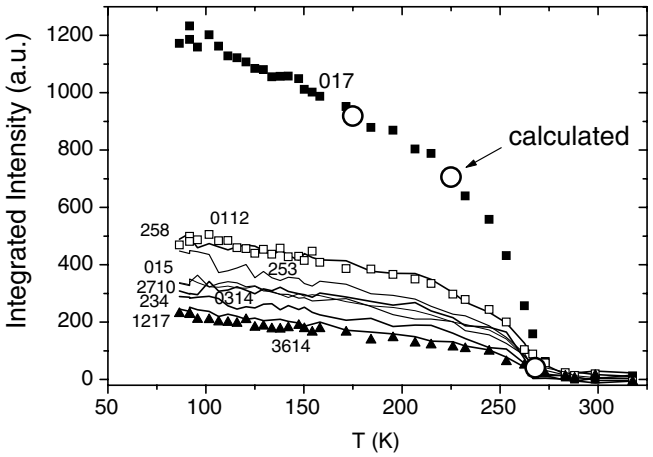

Fig. 1. Temperature dependences of the integrated intensities of selected superstructure peaks. Large open circles correspond to the calculated intensities using temperature dependent atomic positions (Meyer *et al.*, 2001).

One clearly finds a decrease of the integrated intensities with increasing temperature – due to the decrease of the (long range) order parameter – but the intensities do not approach zero at T_c. Above T_c a nonlinear temperature variation is still observed most probably due to short range order effects. This behaviour agrees remarkably with recent excess entropy data measured by conduction calorimetry (Hayward *et al.*, 2002; Martin-Olalla *et al.*, 2001) (Fig. 6) and also with the birefringence data (Fig. 2 of Sondergeld *et al.* (2000)).

To examine the short range order in more detail we performed ω-scans around the ten superstructure peaks as a function of temperature. As an example, Fig. 3 shows

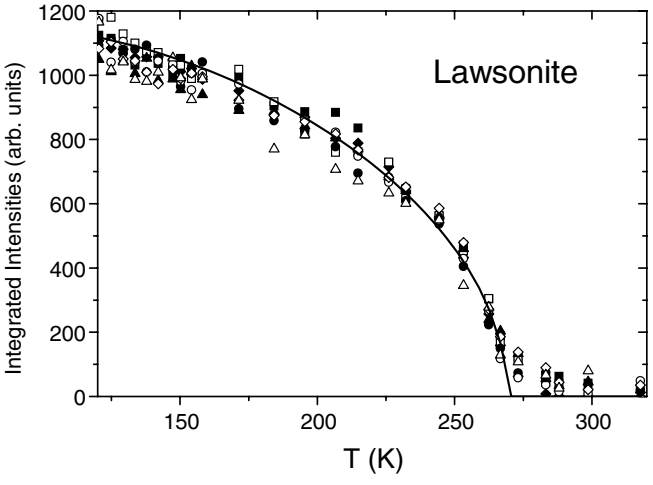

Fig. 2. Temperature dependences of integrated superstructure peak intensities normalized at $T = 150$ K. The solid line shows a fit with tricritical order parameter behaviour, i.e. $I \propto \eta_0^2$ with Eq. (6).

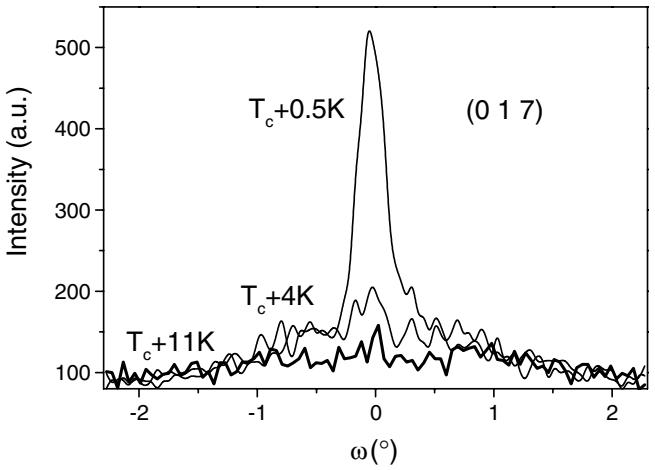

Fig. 3. Temperature evolution of peak profiles of the (0 1 7) superstructure reflection above T_c.

the temperature dependence of the peak profiles of the (017) superstructure reflection above T_c. It displays a clear increase of the diffuse intensity when approaching T_c, whereas the width decreases. Very similar diffuse peaks were also observed for the other superstructure reflections (e.g. Fig. 4).

In Sec. 4 we present a model to describe this behaviour in more detail.

4. Discussion

Let us denote by $2\tau_x = a = 5.847$ Å, $2\tau_y = b = 8.790$ Å, $2\tau_z = 13.128$ Å (Libowitzky *et al.*, 1995) the length of the conventional *Cmcm* base-centered unit cell Γ_0^b. According to Kovalev (1993) the primitive unit cell vectors $\mathbf{a}_1$, $\mathbf{a}_2$ and $\mathbf{a_3}$ are

$$\mathbf{a}_1 = (\tau_x, \tau_y, 0)\,, \quad \mathbf{a}_2 = (-\tau_x, \tau_y, 0)\,, \quad \mathbf{a}_3 = (0, 0, 2\tau_z)$$

and the reciprocal lattice vectors are:

$$\mathbf{b}_1 = \left(\frac{\pi}{\tau_x}, \frac{\pi}{\tau_y}, 0\right); \qquad \mathbf{b}_2 = \left(-\frac{\pi}{\tau_x}, \frac{\pi}{\tau_y}, 0\right);$$
$$\mathbf{b}_3 = \left(0, 0, \frac{\pi}{\tau_z}\right).$$

The phase *Pmcn* belongs to the primitive orthorhombic Bravais lattice type Γ_0, the unit cell of which coincides with the conventional *Cmcm* unit cell and is given by

$$\mathbf{a'}_1 = (2\tau_x, 0, 0)\,, \quad \mathbf{a'}_2 = (0, 2\tau_y, 0)\,, \quad \mathbf{a'}_3 = (0, 0, 2\tau_z)$$

with reciprocal lattice vectors

$$\mathbf{b'}_1 = \left(\frac{\pi}{\tau_x}, 0, 0\right); \qquad \mathbf{b'}_2 = \left(0, \frac{\pi}{\tau_y}, 0\right);$$
$$\mathbf{b'}_3 = \left(0, 0, \frac{\pi}{\tau_z}\right).$$

The transition *Cmcm* → *Pmcn* is associated with an instability at the wave-vector $\mathbf{k}_c = \mathbf{k}_{15} = (\mathbf{b}_1 + \mathbf{b_2})/2$ (here and below in Kovalev's (1993) notation). In terms of the reciprocal lattice vectors $h\mathbf{b'}_1 + k\mathbf{b'}_2 + l\mathbf{b'}_3$ of the *Pmcn*-phase this leads to the condition '$h + k = 2n + 1$' for the superstructure peaks. The star of the wavevector consists of a single vector and all space-group irreducible representations in this point of the Brillouin zone are real and one-dimensional. The one component order parameter η for this transition transforms according to the irreducible representation $\mathbf{T}_3$.

Spatial fluctuations in η give rise to nonzero order parameter Fourier components $\eta(\mathbf{k})$. The cross section for X-rays for a wave-vector transfer $\mathbf{K}$ is given in the one-phonon approximation as (Cowley, 1980)

$$\frac{\mathrm{d}\sigma(\mathbf{K})}{\mathrm{d}\Omega} = |F(\mathbf{K})|^2 \langle\eta\rangle^2 \Delta(\mathbf{K} + \mathbf{k}_c) + \sum_k |F(\mathbf{K})|^2 \langle\eta(\mathbf{k})\,\eta(-\mathbf{k})\rangle_\mathbf{c} \Delta(\mathbf{K} + \mathbf{k_c} + \mathbf{k}) \tag{1}$$

$\Delta(K) = V_B \sum_\tau \delta^{(3)}(\mathbf{K} - \tau)$ where the summation is over the reciprocal lattice vectors τ of the high symmetry phase and $\delta^{(3)}(\mathbf{K})$ is the three-dimensional delta function. V_B is the volume of the Brilouin zone. The connected correlation function $\langle\eta(\mathbf{k})\,\eta(-\mathbf{k})\rangle_c = k_B T\chi(\mathbf{k})$ is proportional to the wave-vector dependent order parameter susceptibility (Cowley, 1980). The influence of the Debye-Waller factor on the X-ray intensities is neglected, since the corresponding temperature variation of the intensity is below 1% between 130 K and T_c (Meyer *et al.*, 2001). The first contribution to Eq. (1) represents the superstructure intensitiy which is proportional to the square of the long range order parameter $\langle\eta\rangle$. The second part describes the evolution of short range order. In interpreting experimental data, a possible weak $\mathbf{K}$-dependence of the structure factors $F(\mathbf{K})$ in Eq. (1) is usually neglected, which yields

$$I_{\mathrm{int}} = \frac{V}{(2\pi)^3} \int\limits_{|K| \le k_m} \frac{\mathrm{d}\sigma(\mathbf{K})}{\mathrm{d}\Omega}\, d^3K = |F|^2 \left(\langle\eta\rangle^2 + \frac{V}{(2\pi)^3} \int\limits_{|K| \le k_m} \langle\eta(\mathbf{k})\,\eta(-\mathbf{k})\rangle_c\, d^3k\right) \tag{2}$$

for the integrated intensity inside the experimental integration window given by $\pm k_m$ in $\mathbf{k}$-space. In the present case, we have $k_m = 0.3 \times 10^{10}$ m^{-1}. Letting k_m approach π/a (a = average lattice constant), the last line of this formula approaches the thermal expectation value $|F|^2 \langle\eta^2\rangle = |F|^2 (\langle\eta\rangle^2 + \langle\eta^2\rangle_c)$. Note that this function is also probed by measuring linear birefringence or excess entropy. In fact it was derived in several works (Sondergeld *et al.*, 2000; Schäfer and Kleemann, 1985) that

$$\delta\,\Delta n_{ij} = \frac{n_0^3}{2}\,(c_i - c_j)\,\langle\eta^2\rangle \tag{3}$$

where n_0 is the average high temperature refractive index and the constants c_i denote the elasto-optic coefficients. Quite similar the excess entropy ΔS reads (Hayward *et al.*, 2002; Ivanov *et al.*, 1990)

$$\Delta S = \frac{A_0}{2}\,\langle\eta^2\rangle \tag{4}$$

where A_0 is the quadratic coefficient of a suitable Landau expansion (see below).

4.1 Mean field approach

The Landau-Ginzburg free energy density of a one-component order parameter system can – with the assumption of isotropic fluctuations – be written as

$$\Phi = \frac{A(T)}{2}\,\eta^2 + \frac{B}{4}\,\eta^4 + \frac{D}{6}\,\eta^6 + \frac{g}{2}\,(\nabla\eta)^2\,. \qquad (5)$$

Including quantum saturation (Salje *et al.*, 1991)) $A(T) = A_0\Theta_s\left[\coth\left(\frac{\Theta_s}{T}\right) - \coth\left(\frac{\Theta_s}{T_0}\right)\right]$, where the value of $\Theta_s = 258$ K was found for the $Cmcm - Pmcn$ transition of Lawsonite (Carpenter *et al.*, 2003). This yields a temperature dependence

$$\eta_0(T) = \sqrt{\frac{-B}{2D} + \sqrt{\frac{B^2}{4D^2} + \frac{A(T)}{D}}} \qquad (6)$$

of the equilibrium order parameter and a wave-vector dependent susceptibility

$$\chi^{-1}(\mathbf{k}) = A(T) + 3B\eta_0^2 + 5D\eta_0^4 + gk^2\,. \qquad (7)$$

The characteristic saturation of the order parameter or properties that depend on coupling to the order parameter occurs at $T \approx \Theta/2$. In fact Fig. 2 shows this leveling off of the order parameter at low temperatures (≈120 K). For the limiting case of a pure order/disorder transition the standard Bragg-Williams model predicts a similar saturation of the order parameter. It was however shown (Carpenter *et al.*, 2003), that the modified Landau solution (6) gives a significantly better fit to the spontaneous strain data for the $Cmcm - Pmcn$ transition.

Since we are here mainly interested in the temperature region near T_c we can safely neglect the low temperature saturation in the following analysis. Then with $A(T) = A_0(T - T_0)$ the transition temperature T_c is determined as $T_c = T_0 + \frac{3}{16}\frac{A_0^2}{BD}$ for $B < 0$ and $T_c = T_0$ for $B \geq 0$. Introducing the correlation length $\xi(T)$ of the order parameter fluctuations

$$\xi(T) = \sqrt{\frac{g}{A_0(T - T_0) + 3B\eta_0^2 + 5D\eta_0^4}} \qquad (8)$$

the **k**-dependent susceptibility takes the simple Lorentzian form

$$\chi(\mathbf{k}) = \frac{\chi(0)}{1 + k^2\xi^2}\,. \qquad (9)$$

The mean square deviation of the order parameter from the mean field value (6) can be written as (Ivanov *et al.*, 1990)

$$\begin{aligned}\langle\eta(T)^2\rangle_c &= \frac{Vk_BT}{(2\pi)^3}\int\limits_{|\mathbf{k}|\leq k_m} d^3k\chi(\mathbf{k}) \\ &= \frac{k_BTk_m}{2\pi^2}\,\frac{\chi(0)}{\xi^2}\left(1 - \frac{\arctan\,(k_m\xi)}{k_m\xi}\right) \\ &\approx k_BT_c\left(\frac{k_m}{2\pi^2 g} - \frac{\sqrt{A_0(T - T_c)}}{4\pi g^{3/2}}\right). \qquad (10)\end{aligned}$$

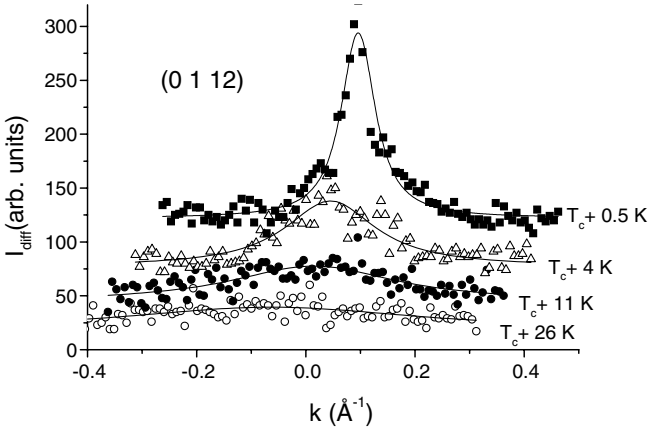

Fig. 4. Evolution of peak profiles (ω scan) of the superstructure reflection (0 1 12) above T_c. The solid lines are fits with Eq. (9), implying Lorentzian line shapes.

The last relation holds for temperatures sufficiently close to T_c. It is the origin of the well known square root behaviour of the specific heat, i.e. $C_V \propto (T - T_c)^{-0.5}$ for small fluctuation corrections often referred to as classical critical behaviour. More specifically, numerical evaluation of Eq. (10) reveals that the specific heat exponent α varies from 0.5 (at temperatures where $k_m\xi \gg 1$) to 1 (for $k_m\xi \ll 1$). This variation of the classical critical exponent α should be taken into account when fitting experimental data in a wide temperature range. A fit of the diffuse scattering peaks (Fig. 4) with Eq. (9) yields the temperature dependence of the correlation length ξ and the peak intensity I_0 (Fig. 5).

From the high temperature correlation length $\xi^2(T > T_c) = \frac{g}{A_0(T - T_c)}$ and the fixed set of Landau coefficients $A_0 = 1.18 \times 10^5$ N/m^2 K, $B = 0$, $C = 3.19 \times 10^7$ N/m^2 reported (Carpenter *et al.*, 2003), a gradient coefficient $g = 4 \times 10^{-13}$ N is determined (Fig. 5). It should be noted that the fits have been performed for all measured superstructure peaks. The fits of the integrated intensities of all superstructure peaks yield the same values for A_0, B, C. Evaluation of the peak profiles of all the diffuse scattering peaks yield gradient coefficients which

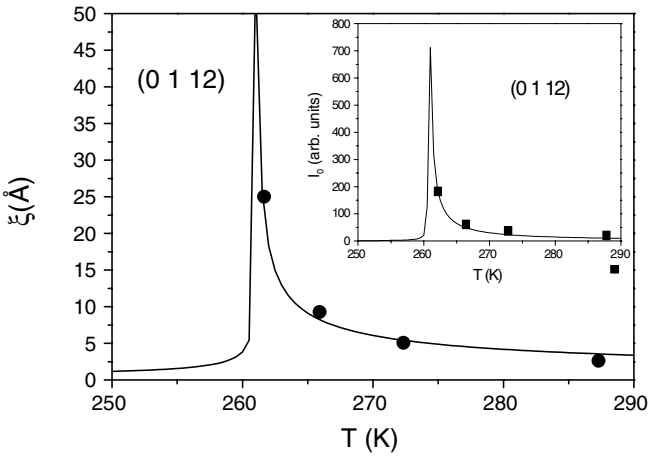

Fig. 5. Temperature dependence of the peak intensity (inset) and the correlation length determined from the HWHM of the (0 1 12) superlattice reflection. The lines are fits with Eqs. (7) and (8).

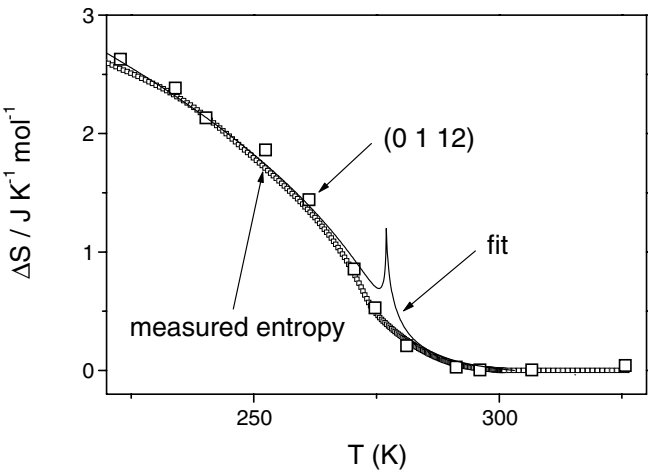

Fig. 6. Temperature dependence of the integrated intensity of the (0 1 12) superstructure reflection (open squares). Full squares show the excess entropy data of Hayward *et al.* (2002). The solid line is a mean field fit of the integrated intensity (2) using Eqs. (6) and (10).

are all of the same order of magnitde (i.e. they vary between 2×10^{-13} N and 6×10^{-13} N). With these parameters we reach the following conclusion: In accordance with Carpenter *et al.* (2003) and also Hayward *et al.* (2002) we are able to obtain good fits of the data in the low symmetry phase as long as the close vicinity ($\approx$3 K) of T_c is excluded. Using such an approach the phase transition indeed looks like being of a *tricritical* type (see full line in Fig. 2).

Nevertheless – as is obvious from Fig. 6 – a more rigorous attempt of course calls for a consistent fit of the whole curve. According to Eqs. (2)–(4) we are forced to find a simulateneous fit of the fluctuation tails above T_c and the long range order below T_c using a single set of parameters, as both components are due to the same order parameter correlation function. It turns out that – within standard Landau -Ginzburg theory – any attempt to produce such large fluctuation tails using the above (or any other physically reasonable) set of parameters necessarily yields a pathologic peak around T_c (cf. the full thin line in Fig. 6). As the fluctuations become comparable to the mean field contribution, a theory including small fluctuation corrections is simply inappropriate to account for the crossover to the critical region. In other words, we observe the violation of the well-known Levanyuk-Ginzburg criterion (Levanyuk, 1959; Ginzburg, 1961), which yields a qualitative estimate of the breakdown of the classical theory.

4.2. Crossover behaviour

As a rule, it is usually prohibitly difficult to experimentally detect the true scaling behaviour of observables around the critical point of a second order phase transition. Often, the scaling region turns out to be extremely narrow and even weak disturbances considerable blur the picture. On the other hand, in order to obtain reliable information concerning the critical point from measurements which are usually taken somewhat outside the critical region, we obviously depend on a profound understanding of the the crossover from mean field to critical behaviour. Consequently, the crossover regime, already recognized to be important by Bruce (1980) is regarded to be extremely relevant from an experimental point of view (Lujten and Binder, 1998; Belyakov and Kiselev, 1992; Anisimov *et al.*, 1992). In fact, several groups have intensified its investigation during the last decade, but a detailed calculation of the thermodynamic crossover functions, i.e. the effective critical exponents was performed rather recently. Specifically, for 3d Ising systems we now know how the effective exponents γ_{eff} (Luijten and Binder, 1998) and α_{eff} (Belyakov and Kiselev, 1992) change from the classic limit to their Ising value when approaching the critical point, while the 2d Ising case was investigated in (Luijten *et al.*, 1997). Both theoretically and numerically the observables were found to follow a scaling behavior with *effective* (i.e. τ-dependent) critical exponents (Kouvel and Fisher; 1964), continuously changing from their mean field values to the asymptotic limit for $\tau \to 0$, where as usual $\tau = |T - T_c|/T_c$. For example, in a 3d Ising system one finds that continuously $\alpha_{\text{eff}}(\tau \to 0)$: $0.5 \to 0.11$ and $\gamma_{\text{eff}}(\tau \to 0)$: $1 \to 1.24$.

Theoretically, the crossover behavior is governed by the parameter τ/G, where G the so called *Ginzburg number* (Anisimov *et al.*, 1992) actually determines the temperature range for which fluctuation contributions start to dominate over the mean-field anomalies. For $\tau/G \ll 1$ asymptotic critical behaviour occurs, whereas classical critical behaviour is expected for $\tau/G \gg 1$. It is well known that G strongly depends on the interaction range of the material. E.g. for ferroelectrics, where long range dipole-dipole interactions exist, the Ginzburg number can take on values as small as 10^{-12} to 10^{-14} (Anisimov *et al.*, 1992), which implies that classical Landau theory is applicable with high accuracy up to the phase transition temperature. As already mentioned above, the low temperature ferroelectric phase transition at $T_2 = 120$ K in lawsonite falls under this category.

For nonferroelectric structural phase transitions it was shown (see e.g. Strukov and Levanyuk, 1998) that the Ginzburg number can be calculated from

$$G = \frac{k_B^2}{64\pi^2 \xi_0^6 (\Delta C_p^L)^2} \tag{11}$$

where $\xi_0 = \sqrt{g/A_0 T_c}$ is the MF correlation length at $T = 0$ K and ΔC_p^L denotes the heat capacity jump at T_c as computed from Landau theory. Using the parameter values gathered above we obtain $\xi_0 \approx 1.4 \times 10^{-10}$ m and with $\Delta C_p^L \approx 0.3$ J/K $\cdot$ g (Martin-Olalla *et al.*, 2001) we calculate a Ginzburg number of $G \approx 0.05$ for the antiferrodistortive phase transition in lawsonite.

Although only computed from an order of magnitude estimation, in the antiferrodistortive case the value of G is clearly much larger than that found for the ferroelectric transition, which provides an explanation of the different character of both transitions. Since symmetry fixes the order parameter of the phase transition *Cmcm* $\to$ *Pmcn* to be scalar, we are led to compare our data to the crossover behavior found for the 3d-Ising universality class. As already mentioned above, the corresponding crossover from classical to the asymptotic critical region was studied nu-

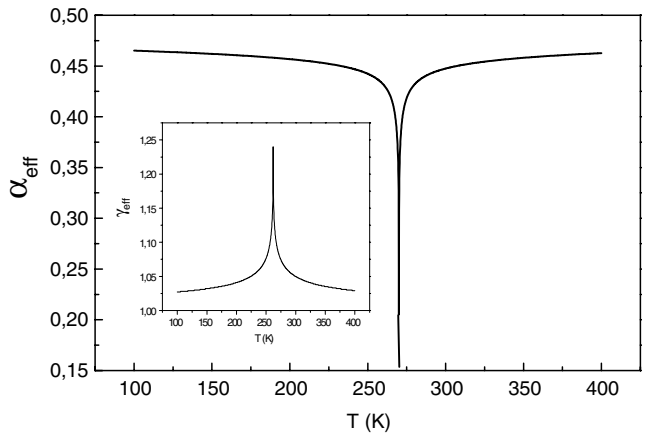

Fig. 7. Crossover behaviour of the effective specific heat exponent for $G = 0.01$.

merically (Luijten and Binder, 1998; Luijten *et al.*, 1997) and by analytical methods, like renormalization group matching (see e.g. Anisimov *et al.*, 1992) and ε-expansions (Belyakov and Kiselev, 1992) or 3-dimensional field theory (Bagnuls and Bervillier, 1985). All these methods lead to very similar results.

To analyze the temperature variation of the entropy or birefringence in terms of the crossover model one introduces the effective (i.e. τ-dependent) critical exponent

$$\alpha_{\text{eff}}(\tau) = -\frac{d \log \Delta\tilde{C}_V(\tau)}{d \log \tau} \tag{12}$$

where $\tilde{C}_V$ denotes a suitably normalized specific heat. One observes that α_{eff} changes from the classical $\alpha_{cl} = 0.5$, to the asymptotic critical value $\alpha = \alpha_{\text{eff}}(0)$ when approaching T_c. For the 3d-Ising model in the asymptotic critical region the exponent $\alpha = 0.11$ and the amplitude ratio $C^+/C^- = 0.465$ is found using e.g. the field-theory approach (Le Guillou and Zinn-Justin, 1980). By use of ε-expansions, Belyakov and Kiselev (1992) show that the full function $\alpha_{\text{eff}}(\tau)$ can be calculated from the implicit equation

$$\tilde{C}_V(t) = \tilde{C}_V^0 - 1 + [1 + 3x(t)^{-1/2}]^{1/3}\,. \tag{13}$$

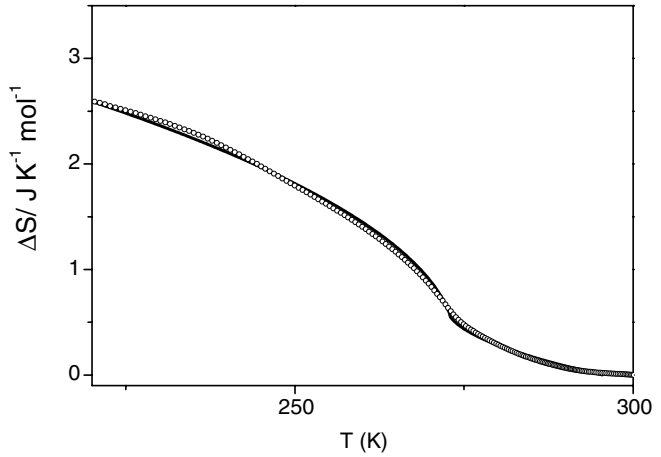

Fig. 8. Temperature dependences of the excess entropy. The line is calculated from the crossover model.

Here $t = \tau/G$, $x = \tilde{\chi}^{-1}/G$ corresponds to the inverse normalized susceptibility and $\tilde{C}_V^0$ is a regular background. It is well known that this crossover function yields a value of $\alpha_{\text{eff}}(0) = 0.167$, which is slightly larger than the field theoretic result of 0.11. However as we show below, this difference is not very important for our purposes, since experimentally we could only follow the crossover to values of $\alpha_{\text{eff}}(0) \approx 0.2$. To calculate $x(t) = t^{\gamma_{\text{eff}}}$, we use the relation

$$\gamma_{\text{eff}} = 1 + (\gamma - \gamma_{MF})\,\frac{1}{1 + t^{3/2}} \tag{14}$$

found by Luijten and Binder (1998). Fig. 7 shows the effective susceptibility and specific heat exponents obtained from Eqs. (14) and (13), respectively.

To determine the crossover behaviour of the excess entropy or birefringence, recall that in the vicinity of T_c the proportionality $\dfrac{\mathrm{d}\delta\, S}{\mathrm{d}\tau}$, $\dfrac{\mathrm{d}\delta\, \Delta n}{\mathrm{d}\tau} \propto \Delta\tilde{C}_V$ holds.

Inserting the temperature dependence of the effective exponent α_{eff} of Fig. 7, we fit the temperature derivative of the excess entropy and birefringence (inset of Fig. 9) as well as the integrated intensity up to T_c. Fig. 8 shows that the resulting excess entropy is excellently reproduced using the values $C_0 = 0.55$ J/Kmol and $C^+/C^- = 0.46$, which is also consistent with the amplitude ratio theoretically calculated for the 3d Ising model (Le Guillou and Zinn-Justin, 1980).

The birefringence curve is also in excellent agreement with the results derived from the model (Fig. 9). It should be noted that the best fits were obtained with $G \approx 0.01$, which agrees – within orders of magnitude – with the value 0.05 calculated above. This implies a crossover interval of a few Kelvin around T_c.

The crossover exponent of the specific heat $\alpha_{eff}(\tau)$ can also be directly calculated from Eq. (12) with $\Delta\tilde{C}_V \propto \dfrac{\mathrm{d}\delta\, \Delta n}{\mathrm{d}\tau}$. Fig. 10 shows, that α_{eff} varies from $\approx$0.2 near T_c to $\approx$1 away from T_c, which agrees excellently with the crossover model (inset of Fig. 10) if the full form of Eq. (10) is taken into account.

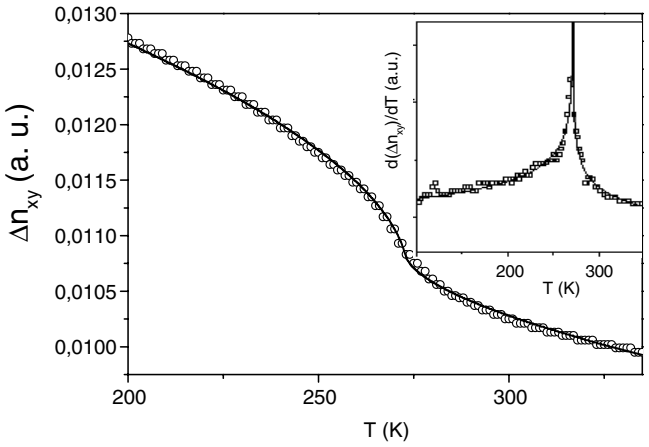

Fig. 9. Temperature dependence of the birefringence component Δn_{xy}. The line is calculated from the crossover model. The inset shows the variation of the isochoric specific heat calculated from the birefringence data.

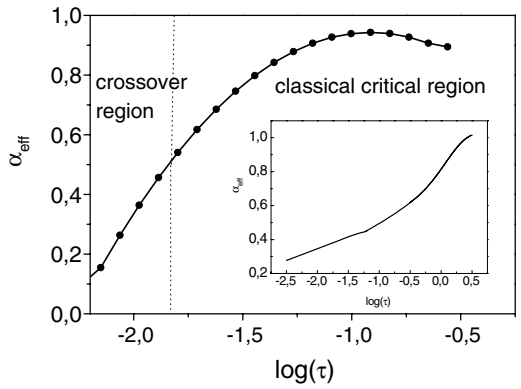

Fig. 10. Crossover behaviour of the effective specific heat exponent calculated from the experimental birefringence data. The inset shows the theoretical behaviour of α_{eff} following from Eq. (10).

5. Summary and discussion

Our analysis of X-ray, birefringence and entropy measurements in the vicinity of the antiferrodistortive phase transition at $T_c = 270$ K of lawsonite single crystals yields the following main results: From the data the temperature dependence of the long range order parameter is extracted and fitted to a tricritical power law in a large temperature range $[T_c - 120\,\mathrm{K},\ T_c - 3\,\mathrm{K}]$. In the high symmetry phase huge pre-transitional effects are observed in excess entropy, strain tensor components, X-ray intensities and birefringence. These tails were found to extend up to about 200 K above T_c. Simultaneously, diffuse scattering peaks centered at the critical wavevector were measured. In principle, two different origins for such precursor tails may be envisaged, namely extrinsic order parameter fluctuations due to defects or intrinsic (thermal) order parameter fluctuations. It is very difficult to disentangle both effects and in principle one could have them both superimposed. Nevertheless, there are several arguments contradicting a strong influence of defects on the precursor tails found in lawsonite. First of all, the chemical composition of the measured samples was determined to be close to the ideal one (see Sec. II.A.). Moreover, samples with slightly varying composition and from different sources show practically identical thermodynamic properties, i.e. tricritical behaviour and similar high temperature tails. In addition, the ferroelectric phase transition to the $P2_1cn$-phase at $T_2 = 120$ K is not accompanied by any high temperature tails (Carpenter *et al.*, 2003), or other significant rounding effects (Sondergeld *et al.*, 2000; Sondergeld *et al.*, 2001). Indeed, X-ray (Sondergeld *et al.*) and dielectric (Sondergeld *et al.*, 2001) measurements indicate that the ferroelectric phase transition in lawsonite can be very well described by a classical 2–4 Landau potential. It is hard to believe that a small amount of defects would only influence the antiferrodistortive phase transition while still being invisible to the ferroelectric one.

The antiferrodistortive phase transition really appears to be of second order. In fact, the coupling between the order parameter and the strain components is very small, the dip anomalies in the longitudinal elastic constants being smaller than 3% at T_c (Sondergeld *et al.*). To account for the effects of intrinsic order parameter fluctuations, we applied the following approach: Based on a Landau-Ginzburg model (Ginzburg, 1961) in mean-field approximation we have determined the coefficients of the Landau-Ginzburg free energy from the excess entropy and X-ray data. With these parameters one can fit the data in a broad temperature range except of a narrow region near T_c. In this temperature range the fluctuation tails start to approach the value of the spontaneous (long range) part of the order parameter, i.e. the system is clearly leaving the classical region. However, as we have shown above, in this temperature regime we were able to consistently fit our data using theoretically predicted crossover functions for the effective critical exponents and the corresponding amplitude ratios. Application of the Ginzburg-Levanyuk criterion shows that the crossover from classical to asymptotic critical behaviour starts some Kelvin away from T_c. This relatively large temperature interval can be understood as an effect of the short range interactions which drive the antiferrodistortive phase transition in lawsonite. However, this does by no means imply that it is comparable to the temperature range of the true asymptotic critical region. Indeed, while we have demonstrated that the onset and development of the crossover can be clearly followed, the asymptotic critical region is expected to still be orders of manitude smaller and may not be directly observable at all.

Acknowledgments. We would like to thank Zsolt Revay and Gabor Molnar for kindly carrying out the Prompt Gamma Activation Analysis (PGAA) of our samples at the Budapest Neutron Center (BNC). We are grateful to K. Parlinski, J. M. Perez-Mato and Ch. Dellago for very helpful discussions. The present work was performed in the frame of the EU Network on Mineral Transformations (contract no. ERB-FMRX-CT97-0108).

References

Anisimov, M. A.; Kiselev, S. B.; Sengers, J. V.; Tang, S.: Crossover approach to global critical phenomena in fluids. Physica A**188** (1992) 487–525.

Bagnuls, C.; Bervillier, C.: Nonasymptotic critical behavior from field theory at $d = 3$: The disordered-phase case. Phys. Rev. B**32** (1985) 7209–7231.

Baur, W. H.: Crystal structure refinement of lawsonite. Am. Mineral. **63** (1978) 311–315.

Belyakov, M. Y.; Kiselev, S. B.: Crossover of the susceptibility and the specific heat near a second-order phase transition. Physica A**190** (1992) 75–94.

Bruce, A. D.: Structural phase transitions. II. Static critical behaviour. Adv. Phys. **29** (1980) 111–217.

Carpenter, M. A.; Meyer, H. W.; Sondergeld, P.; Marion, S.; Knight, K. S.: Spontaneous strain variations through the low-temperature phase transitions of deuterated lawsonite. Am. Mineral. **88** (2003) 534–546.

Cowley, R. A.: Structural phase transitions. I. Landau theory. Adv. Physics **29** (1980) 1–110 .

Ginzburg, V. L.: Some remarks on phase transitions of the second kind and the microscopic theory of ferroelectric materials. Sov. Phys. Solid State **2** (1961) 1824–34.

Hayward, S.; Burriel, R.; Marion, S.; Meyer, H. W.; Carpenter, M. A.: Kinetic effects associated with the low temperature phase transitions in lawsonite. Eur. J. Min. **14** (2002) 1145–53.

Ivanov, N. R.; Levanyuk, A. P.; Minyukov, S. A.; Kroupa, J.; Fousek, J.: The critical temperature dependence of birefringence near the normal-incommensurate phase transition in Rb_2ZnBr_4. J. Phys.: Condens. Matter **2** (1990) 5777–5786.

Kim, Y. C.; Anisimov, M. A.; Sengers, J. V.; Luijten, E.: Crossover Critical Behavior in the Three-Dimensional Ising Model. J. Statist. Phys. **110** (2003) 591–609.

Kouvel, J. S.; Fisher, M. E.: Detailed Magnetic Behavior of Nickel Near its Curie Point. Phys. Rev. **136** (1964) A1626–A1632

Kovalev, O. V.: Representation of the Crystallographic Space Groups. (Eds.) H. T. Stokes and D. M. Hatch, Gordon and Breach Science Publishers, p. 390 (1993).

Le Guillou, J. C.; Zinn-Justin, J.: Critical exponents from field theory. Phys. Rev. B **21** (1980) 3976–3998.

Levanyuk, A. P.: Contribution to the theory of light scattering near the second-order phase-transition points. Sov. Phys. JETP **9** (1959) 571–576.

Libowitzky, E.; Ambruster, T.: Low-temperature phase transitions and the role of hydrogen bonds in lawsonite. Am. Mineral. **80** (1995) 1277–1285.

Libowitzky, E.; Rossman, G. R.: FTIR spectroscopy of lawsonite between 82 and 325 K. Am. Mineral. **81** (1996) 1080–1091.

Luijten, E.; Blöte, W. J.; Binder, K.: Nonmonotonic Crossover of the Effective Susceptibility Exponent. Phys. Rev. Lett. **79** (1997) 561–564.

Lujten, E.; Binder, K.: Nature of crossover from classical to Ising-like critical behaviour. Phys. Rev. E**58** (1998) 4060–4063.

Martin-Olalla, J. M.; Hayward, S. A.; Meyer, H. W.; Ramos, S.; del Cerro, J.; Carpenter, M. A.: Phase transitions in lawsonite: a calorimetric study. Eur. J. Min. **13** (2001) 5–14.

Meyer, H. W.; Marion, S.; Sondergeld, P.; Carpenter, M. A.; Knight, K. S.; Redfern, S. A. T.; Dove, M.: Displacive components of the low-temperature phase transitions in lawsonite. Am. Mineral. **86** (2001) 566–577.

Salje, E. K. H.; Wruck, B.; Thomas, H.: Order parameter saturation and low-temperature extension of Landau theory. Z. Physik B: Condensed Matter **82** (1991) 399–404.

Schäfer, F. J.; Kleemann, W.: High-precision refractive index measurements revealing order parameter fluctuations in $KMnF_3$ and NiO. J. Appl. Phys. **57** (1985) 2606–2611.

Schmidt, M. W.: Lawsonite: upper pressure stability and formation of higher density hydrous phases. Am. Mineral. **80** (1995) 1286–1292.

Schmidt, M. W.; Poli, S.: Experimentally based water budgets for dehydrating slabs and consequences for arc magma generation. Earth Planetary Sc. Lett. **163** (1998) 361–379.

Sondergeld, P.; Schranz, W.; Tröster, A.; Carpenter, M. A.; Libowitzky, E.; Kityk, A. V.: Optical, elastic and dielectric studies of the phase transitons in Lawsonite. Phys. Rev. B **62** (2000) 6143–6147.

Sondergeld, P.; Schranz, W.; Tröster, A.; Kabelka, H.; Meyer, H.; Carpenter, M. A.; Lodziana, Z.; Kityk, A. V.: Dielectric relaxation and order parameter dynamics in lawsonite. Phys. Rev. B**64** (2001) 241051–241056.

Sondergeld, P.; Schranz, W.; Armbruster, T.; Giester, G.; Kityk, A. V.; Carpenter, M. A.: Ordering and elasticity associated with the low-temperature phase transitions in lawsonite. Am. Mineral. **90** (2005) 448.

Strukov, B. A.; Levanyuk, A. P.: Ferroelectric Phenomena in Crystals. Springer-Verlag (1998) p. 125.

Zimmermann, M.; Schranz, W.: A "hybrid" apparatus for automatic birefringence measurements. Meas. Sci Technol. **4** (1993) 186–189.